 MCB, vol.7, no.3, pp.175-192, 2010

Discrete Element Analysis in Musculoskeletal Biomechanics

Chao EYS[*], Volokh KY[†], Yoshida H[‡], Shiba N[§] and Ide T[¶]

Abstract: This paper is written to honor Professor Y. C. Fung, the applied mechanician who has made seminal contributions in biomechanics. His work has generated great spin-off utility in the field of musculoskeletal biomechanics. Following the concept of the Rigid Body-Spring Model theory by T. Kawai (1978) for non-linear analysis of beam, plate, and shell structures and the soil-gravel mixture foundation, we have derived a generalized Discrete Element Analysis (DEA) method to determine human articular joint contact pressure, constraining ligament tension and bone-implant interface stresses. The basic formulation of DEA to solve linear problems is reviewed. The derivation of non-linear springs for the cartilage in normal diarthrodial joint contact problem was briefly summarized. Numerical implementation of the DEA method for both linear and non-linear springs is presented. This method was able to generate comparable results to the classic contact stress problem (the Hertzian solution) and the use of Finite Element Modeling (FEM) technique on selected models. Selected applications in human knee and hip joints are demonstrated. In addition, the femoral joint prosthesis stem/bone interface stresses in a non-cemented fixation were analyzed using a 2D plane-strain approach. The DEA method has the advantages of ease in creating the model and reducing computational time for joints of irregular geometry. However, for the analysis of joint tissue stresses, the FEA technique remains the method of choice.

[*] Orthopaedic Biomechanics Laboratory, Johns Hopkins University, Baltimore, Maryland 21205-2196. Corresponding author. 9114 Filaree Ct., Corona, CA 92883; E-mail: eyschao@yahoo.com

[†] Department of Civil & Environmental Engineering, Technion - Israel Institute of Technology, Haifa, Israel

[‡] Department of Mechanical Engineering, Shinshu University, Shinshu, Japan

[§] Department of Orthopaedic Surgery, Kurume University School of Medicine, Kurume, Japan

[¶] Department of Orthopaedic Surgery, Yamanashi University School of Medicine, Yamanashi, Japan

1 Introduction

Musculoskeletal biomechanics in its classical sense is a branch of applied mechanics with its main goal of determining the motion, forces, interfacial and internal stress/strain of the system including all the connective tissues and artificial replacement parts engaged in functional activities. Unfortunately, after nearly three decades of intensive effort, much of the useful biomechanical data related to the system in normal, diseased and surgically reconstructed states are either incomplete, inaccurate or unavailable due to a variety of reasons not all of that are technical. The order of determining this biomechanical information is important. In other words, before knowing the realistic loading conditions applied to the system and the material properties of the connective tissue involved, determination of joint contact pressure and tissue stress/strain would be impractical and misleading at times. More concerning at the present time is the unusual enthusiasm in pursuing the micro and nano-mechanics at the cellular and molecular level without adequate knowledge of how the global and system loading is transmigrated to the sub-cellular environment surrounded by medias of unknown behavior and their chemical and electro-physical interactions at different cascades of tissue transition.

In dealing with biomechanical problems involving the musculoskeletal joint system, to obtain closed-form analytical solution in different types of models and analysis is often very difficult if not impossible. Moreover, to study human articular joint contact problem encountered several technical challenges not easily resolved (Shi et

al., 1993). The irregular joint geometry and the complex non-linear physical properties of the articular cartilage have made these problems more difficult. The finite element method (FEM) has been utilized with good success but the tedious modeling process and lengthy computational time prevented it from practical applications where rapid solution turn-around is required. When only the joint contact area/pressure and ligament tension data is required, efficient and reliable modeling and computational methods are highly desirable. To meet these requirements, the Rigid Body-Spring Model (RBSM) technique approach developed by Kawai and Toi (1978) is most ideal and easy to implement. Since the RBSM uses discrete elements of finite dimension to simulate the rigid bodies in contrast to FEM, a new term of Discrete Element Analysis (DEA) was defined to differentiate these two methodologies (Shuind et al., 1995). In performing preoperative planning or custom implant design for individual patient, the joint geometry, skeletal dimension, and the functional demands are different, DEA method will meet these requirements and able to produce the specific data needed for clinical decision making purposes.

After nearly two decades of intensive work in the field of inelastic analysis of steel and concrete structures, Kawai recapitulated the concept of the Rigid Body-Spring Model (RBSM) technique (1980). This technique was based on the "slip line theory" in plasticity in that slip lines connect rigid bodies between which the dilatational and sliding (shear) movements occur. The nodes of such discrete rigid elements are at their respective body centroids, the superposition of element nodes does not exist. Although there are simplifications on these elements and their interconnectivity, the solutions obtained in elastoplastic analysis are quite good. Application of this method was successful in determining the collapse load in metal and concrete beam, plate, or shell structures, in analyzing shift and deformation of underground tunnels, soil-gravel mixture dams and foundations, and in studying incompressible viscous fluid flow problems involving discrete media (Kawai and Watanabe, 1984).

Working closely with several orthopaedic surgeons in Japan, Kawai derived a simple 2D discrete element analysis to study the contact area/pressure and instability of human normal and deformed hip joint (Ide et al., 1989, 1991; Shiba, 1991). This method was expanded to study the knee, shoulder, elbow, wrist and hand joints with great success (An et al., 1990; Horii et al., 1990; Hsu et al., 1990; Shuind et al., 1995; Iwasaki et al., 1998). Since each joint has only two rigid elements, contact pressure and constraining ligament tension can be readily calculated from the deformations of either the compressive or the tensile linear springs placed between the articulating surfaces and around the joint as a function of the applied joint load. Although the number of the springs can be quite large in 3D models, the computational time on an averaged PC computer is insignificant including the iterative process required to converge to the final equilibrium solution. Joint geometry, loading conditions and the spring elastic properties for the cartilage and ligaments (including the capsular structure) can be changed easily for parametric analysis. Micro-movements of the rigid bodies associated with each degree of freedom can be calculated and displayed. Finally, frictional forces in translation and rotation can be incorporated using special shear and torsional springs (Ide et al., 1989).

Using a surface modeling technique to create musculoskeletal models from CT and MRI image data or using the generic cadaveric model's sequential cross-sectional image dataset (Chao, 2003), kinematic analysis of limb movement, determination of muscle and joint loads, calculating joint contact area and pressure plus ligament tension using the DEA technique, and the use of FEM for tissue stress/strain analysis can all be solved in a simulation environment using a generalized custom software containing model building capability, various analysis tools and algorithms, and a virtual laboratory to conduct experiments and parametric investigations. The models can also incorporate bone fracture fixation device and joint prosthetic replacement prosthesis properly integrated to the musculoskeletal system for biomechanical analysis. The study results can be

displayed graphically in an animated fashion together with the model to make them easy to understand and enhance their clinical utility.

This paper will review the basic theory and computational algorithm of the DEA method to solve the contact problems involving multiple rigid bodies. The use of both linear and non-linear springs at the rigid body contact surface will be discussed. Several application examples in musculoskeletal system with relevant clinical significance are presented. Validation of the DEA method was performed using axisymmetric linear elastic contact problem with known solution and by comparing the numerical results from DEA with that generated using the FEM technique in the same model. The application of the quick-modeling technique with simplified DEA analysis and a real-time graphic display of the model and the analysis outcome for pre-operative planning application in orthopaedic surgery are discussed. Although this paper was intended to honor those who have made extraordinary contributions in applied mechanics as well as biomechanics, we sincere hope that our effort will reaffirm the critical importance in pursuing practical biomechanical analysis at the system and tissue level using reliable and effective method to optimize the evidence-based clinical care to patients with musculoskeletal injury, disease and deformity.

2 General theory and formulation of DEA method

Kawai proposed a new discrete model of multiple rigid bodies in contact as shown in Fig. 1. These bodies are considered in equilibrium under external loads denoted by solid arrows and the reaction forces (contact pressure) are produced by the deformation of the inter-positioning springs which are distributed over the contact surfaces of adjacent bodies. In the presentation, the contact area was assumed known but in the development of the actual problem solution algorithm, these contact areas are unknown and they can be determined only by an iterative manner based on the originally assumed contact areas before the external loads are applied. Isolate two of the contacting bodies, an infinitesimal deformation of the interfacial springs is considered (Fig. 2). The displacement vector $\mathbf{u}$ of an arbitrary point in one of the two rigid bodies can be given by the following vector equation:

$$\mathbf{u} = \mathbf{u}_G + \mathbf{O} \times (\mathbf{r} - \mathbf{r}_G) \tag{1}$$

where $\mathbf{u}_G$ is the displacement vector of the body centroid, G, $\mathbf{O}$ is the infinitesimal rotation vector, and $(\mathbf{r} - \mathbf{r}_G)$ is the position vector of an arbitrary point with respect to the centroid before deformation.

$$\mathbf{u} = (u_G, v_G, w_G), \quad \mathbf{O} = (\theta, \phi, \chi) \tag{2}$$

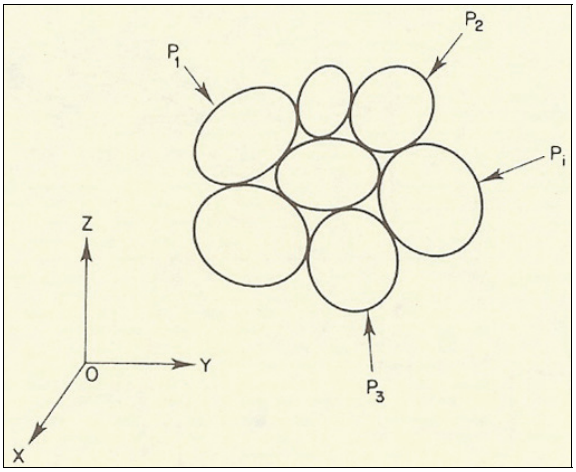

Figure 1: Multiple rigid bodies with elastic surfaces are in contact and equilibrium under external loads, P_1, P_2, P_3 and P_4 for contact area and stress analysis using the Discrete Element Analysis (DEA) technique.

Denoting the displacement vectors of an arbitrary point P(x, y, z) in bodies (I) and (II) by $\mathbf{u}'$, $\mathbf{u}''$, respectively, where

$$\mathbf{u}' = \mathbf{u}_1 + \mathbf{O}_1 \times (\mathbf{r} - \mathbf{r}_1)$$

$$\mathbf{u}'' = \mathbf{u}_2 + \mathbf{O}_2 \times (\mathbf{r} - \mathbf{r}_2)$$

we can write the relative displacement vector of the point P as:

$$P'P'' = \mathbf{u}'' - \mathbf{u}' = \delta(\delta_x, \delta_y, \delta_z) \tag{3}$$

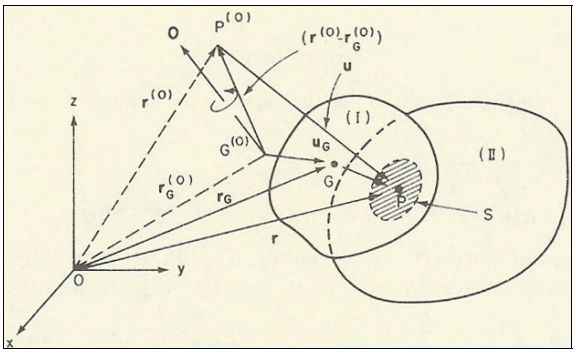

Figure 2: Definition of contact area between bodies I and II in the DEA formulation. **S**: contact area and superscript $^{(0)}$ indicate the state before loading and deformation.

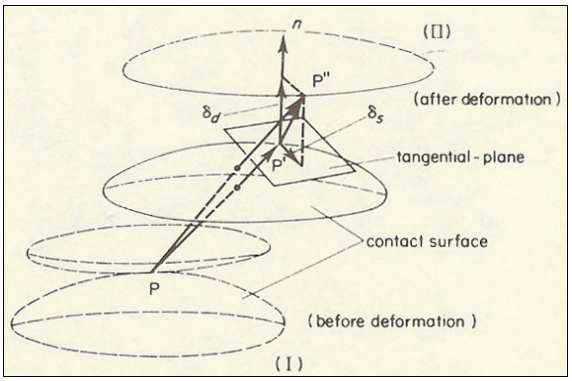

Figure 3: Relative displacement of a point P on the contact surface between bodies I and II.

This relative displacement can also be expressed as (δ_d, δ_s) denoting the normal and transverse displacement components respective to the local coordinates as shown in Fig. 3 where δ_d normal to the surface, S, can be written by

$$\begin{aligned}\delta_d &= (P'P'', \mathbf{n}) \\ &= l(u''-u') + m(v''-v') + n(w''-w'),\end{aligned} \tag{4}$$

where $\mathbf{n} = (l, m, n)$.

Similarly, the transverse displacement δ_s in the tangential plane to the surface can be written as,

$$\begin{aligned}\delta_s^2 =& |\mathbf{n} \times P'P''|^2 \\ =& \{m(w''-w') - n(v''-v')\}^2 \\ &+ \{n(u''-u') - l(w''-w')\}^2 \\ &+ \{l(v''-v') - m(u''-u')\}^2\end{aligned} \tag{5}$$

Based on these preliminary derivations, the strain energy due to the relative displacement (δ_d, δs) of the spring system at point P on the contact surface **S** can be given by

$$V = 1/2 \iint_s (k_d \delta_d^2 + k_s \delta_s^2) d\mathbf{S} \tag{6}$$

From equations (4), (5), the strain energy V is a quadratic function of the displacement vector **u** of the centriods of bodies (I) and (II) which can written as,

$$V(\mathbf{u}) = 1/2 \mathbf{u}^T \mathbf{k} \mathbf{u} \tag{7}$$

where $\mathbf{u}^T = [u_1, v_1, w_1, \theta_1, \phi_1, \chi_1; u_2, v_2, w_2, \theta_2, \phi_2, \chi_2]$.

Based on the small deformation and linear elastic spring assumption, applying the Castigniano's theorem, the following stiffness equation can be derived,

$$\mathbf{R} = \partial V / \partial \mathbf{u} = \mathbf{k} \mathbf{u} \tag{8}$$

Where **k** is a (12×12) symmetric matrix can be written as, $\mathbf{k} = k_{ij,}$ which relate to the displacement components of bodies I and II, and **R** is the nodal reaction vector expressed in terms of the forces and moments,

$$\begin{aligned}&\mathbf{R}^T = \\ &[X_1, Y_1, Z_1, L_1, M_1, N_1; X_2, Y_2, Z_2, L_2, M_2, N_2]\end{aligned} \tag{9}$$

The normal and shear spring stiffness constants (principal components of matrix, **k**) k and k can be determined systematically by using the finite difference expression of the corresponding strain components. On the contact surface **S** shown in Figure 2, the normal and tangential stresses $\boldsymbol{\sigma}_n$, $\boldsymbol{\tau}_{ns}$ satisfy the following expressions,

$$\boldsymbol{\sigma}_n = E' \boldsymbol{\varepsilon}_n, \quad \tau_{ns} = G \gamma_{ns} \tag{10}$$

where

$$E' = (1-\upsilon)E / \{(1+\upsilon)(1-2\upsilon)\}$$

The strain components ε_n and γ_{ns} are expressed by the following finite difference expressions:

$$\boldsymbol{\varepsilon}_n = \delta_d / h, \boldsymbol{\gamma}_{ns} = \delta_s / h \tag{11}$$

where h is the projection of the vector G_1G_2 (G is the centroid of the rigid body) on $\mathbf{n}$. For the specific application dealing with joint contact pressure determination, the definition of spring constants is given,

$$\boldsymbol{\sigma}_n = k_d\delta_d, \quad \boldsymbol{\tau}_{ns} = k_s\delta_s \tag{12}$$

Comparing to equation (10), the normal and shear spring constants between the two contacting rigid bodies are

$$k_d = E'/h, \quad k_s = G/h \tag{13}$$

Knowing the spring constants and the nodal reactions, Eq. (8) will be used to determine the relative displacement of the bodies and thus the normal stress (contact pressure) and shear stress at the contact point. Normally, the contact area, $\mathbf{S}$ (Fig. 2), is subdivided into small areas (ΔS_i) each of which is fitted with the springs defined above. The numerical implementation of the computation required for the contact stresses will be presented at the end of this section.

2.1 Non-linear Spring Model

In the original development of the theory of discrete limit analysis, Kawai and his co-workers did consider spring constant for the opposing rigid elements to be in the plastic range (Kawai, 1977; Kawai and Ito, 1978; Kawai and Takeuchi, 1981). Additionally, system under dynamic loading condition was also discussed by including sliders and dashpots parallel or in series with the springs to model the elasto-visco-plastic problems of solids (Kawai and Toi, 1978). Human joints layered with hyaline cartilage behave in a highly complex manner due to the non-linear articulating material plus its biphasic behavior (Mow and Ratcliffe, 1997). During joint function, the cartilage deforms in three stages – the early stage of instantaneous deformation, the transient stage, and the steady-state stage. During the steady-state stage, the loading is either static or cyclic which will be less affected by the fluid phase of the material and thus making the numerical solution of realistic anatomical joint contact problem more tractable while still able to retain the non-linear property of the cartilage matrix material. With this premise, the non-linear spring was developed for the DEA method for joint contact area/stress analysis for diarthrodial joints (Volokh et al, 2007).

Ateshian et al (1997) and Huang et al (2005) performed experimental and theoretical analyses of the one-dimensional confined compression of articular cartilage. They found that the axial stress-stretch law for non-linear behavior of the specimen could be approximated as follows

$$\sigma = \frac{H_{A0}(\lambda^2-1)}{2\lambda^{2\beta+1}}\exp\{\beta(\lambda^2-1)\}, \tag{14}$$

where σ is the axial Cauchy stress in the solid phase; λ is the axial stretch (other principal stretches equal unity); H_{A0} and β are material parameters. These material parameters can be roughly estimated for the human and bovine articular cartilage: $0.3 \le H_{AO} \le 0.6$; $0.05 \le \beta \le 0.6$.

Based on the analysis of Ateshian et al (1994), we assume that stretches are essentially uniform with depth of the cartilage layer. This allows introducing a non-linear spring with a uniform deformation along its length (or the thickness of the cartilage). Let the average spring force be designated σ and the relative elongation of the spring is $\varepsilon = (h-h_0)/h_0$ where h_0 and h is the cartilage thickness before and after deformation accordingly. Then $\lambda = \varepsilon + 1$ and Eq. (1) takes the form

$$\sigma(\varepsilon) = \frac{H_{A0}((1+\varepsilon)^2-1)}{2(1+\varepsilon)^{2\beta+1}}\exp\{\beta((1+\varepsilon)^2-1)\}. \tag{15}$$

Using this formula, the material parameters are defined for the range $0.05 \le \beta \le 0.6$. The positive values of the relative elongation (engineering strain) and the corresponding stresses are irrelevant, of course, because the springs are unilateral and they do not resist tension. However, the tension of the springs should be taken into account to provide robustness of the computational algorithm described below. The negative values of strains and the corresponding compressive stress are of interest. It is remarkable that the stress-strain curve is almost linear up to 30% strain

while a slight deviation from the linearity emerges in the strain range of 30-40%, i.e. at the limits of the physiologically reasonable values of engineering strain. This observation gives an experimental validation for the classical discrete element analysis based on the linear spring approximation when engineering strains do not exceed 30%. If, however, the strains are about 30% or more the classical discrete element analysis should be modified as follows.

The original form of the non-linear spring definition presented by Eq. (15) can be expressed using power series about$\varepsilon = 0$:

$$\sigma(\varepsilon) = \frac{H_{A0}}{2}(2\varepsilon - \varepsilon^2 + (1+4\beta)\varepsilon^3 + O(\varepsilon^4)). \quad (16)$$

Equations (15) and (16) almost coincide with each other on the segment $-0.4 \leq \varepsilon \leq 0.4$ for the limit values ofβ. The strain energy density of the springs can be readily written as,

$$w(\varepsilon) = \int \sigma(\varepsilon)d\varepsilon = \alpha_1 \frac{\varepsilon^2}{2} + \alpha_2 \frac{\varepsilon^3}{3} + \alpha_3 \frac{\varepsilon^4}{4}, \quad (17)$$

$$\begin{cases} \alpha_1 = H_{A0} \\ \alpha_2 = -H_{A0}/2 \\ \alpha_3 = H_{A0}(1+4\beta)/2 \end{cases} \quad (18)$$

where $w(0) = 0$ was assumed. It is worth noting that h_0 and h in the formulae above denote the cartilage stiffness of two contacting layers in compression. There is no contact when the spring is in tension. This means that deformations with $\varepsilon > 0$ should be excluded from the considerations. The latter can be done by excluding the springs in tension from the contact zone. Changing the contact area iteratively it is possible to find the equilibrium state where all springs within the area of contact are compressed.

3 Numerical Implementation

The finite contact surface between the two adjacent elements before external load is applied can be estimated. In 2D problem, linear springs are distributed per unit length of the estimated contact line usually in the density of 1 spring per mm with the spring fixed at the mid point of the line segment. In order to accommodate the depth of the contact area in 2D model, the spring constant was adjusted according to the depth of the joint (Fig. 4) (Shuind et al., 1995). In 3D problems, the estimated contact surface are divided into finite number of small areas (ΔS_i) bonded by triangular or rectangular meshes at approximately 1 mm^2 per spring density with the spring affixed at the centroid of each area unit. When the deformations of the springs are calculated, the compressive forces, thus the pressure, on the contact surface will be easily determined using the respective elastic constant assigned a priori.

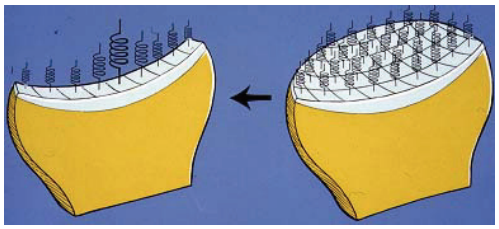

Figure 4: In two-dimensional DEA model, the three-dimensional joint surface contact area depth can be approximated by adjusting the spring stiffness value in pressure calculation.

Using the 3D contact area model with non-linear springs as a general form for numerical implementation, the total energy of the system can be written in the following form,

$$V(\mathbf{u}) = \sum_{i=1}^{N} \Delta S_i \left(\alpha_1 \varepsilon_i^2/2 + \alpha_2 \varepsilon_i^3/3 + \alpha_3 \varepsilon_i^4/4\right) - \mathbf{u}^T \mathbf{R}, \quad (19)$$

where the sum is over N surface elements with area ΔS_i each; ε_i is a relative elongation of the normal spring associated with the ith element; Δl_i is the ith spring elongation and $h_i$is the ith element thickness – spring initial length; α_1, α_2, α_3 are material parameters defined in Eq. (5); $\mathbf{u}$ is a vector of displacements and rotations of the considered rigid bodies expressed in Eq. (7), and $\mathbf{r}$ is vector of the reactive forces and moments, which may include the inertia forces, as given in Eq. (9). The relative displacement δ_i of the ith contact

point (x_i, y_i, z_i) on the boundary surface of bodies 1 and 2 can be expressed as a linear function of the small relative displacements of the bodies

$$\delta_i = \mathbf{B}_i \mathbf{u}, \tag{20}$$

where

$$\mathbf{B}_i = \begin{bmatrix} -1 & 0 & 0 & 0 & -(z_i - z_1) \\ 0 & -1 & 0 & (z_i - z_1) & 0 \\ 0 & 0 & -1 & -(y_i - y_1) & (x_i - x_1) \end{bmatrix}$$
$$\begin{matrix} (y_i - y_1) & 1 & 0 & 0 & 0 \\ -(x_i - x_1) & 0 & 1 & 0 & -(z_i - z_2) \\ 0 & 0 & 0 & 1 & (y_i - y_2) \end{matrix}$$
$$\begin{bmatrix} (z_i - z_2) & -(y_i - y_2) \\ 0 & (x_i - x_2) \\ -(x_i - x_2) & 0 \end{bmatrix} \tag{21}$$

It should not be missed that small displacements of the rigid bodies-bones (as compared to their size) can produce large elongations of springs-cartilage (as compared to their size). Using Eq. (20) it is possible to find the relative spring elongations included in Eq. (19) as follows

$$\varepsilon_i = h_i^{-1} \mathbf{n}_i^T \delta_i = h_i^{-1} \mathbf{n}_i^T \mathbf{B}_i \mathbf{u}, \tag{22}$$

Substituting Eq. (22) in Eq. (19) and applying the minimum energy principle or the Castigniano's theorem, it is possible to get the equilibrium equation

$$\begin{aligned} \mathbf{g}(\mathbf{u}) &= \left(\frac{\partial V}{\partial \mathbf{u}} \right)^T \\ &= \sum_{i=1}^{N} \Delta S_i (\alpha_1 \varepsilon_i + \alpha_2 \varepsilon_i^2 + \alpha_3 \varepsilon_i^3) \left(\frac{\partial \varepsilon_i}{\partial \mathbf{u}} \right)^T - R \\ &= \mathbf{0}, \end{aligned} \tag{23}$$

$$\frac{\partial \varepsilon_i}{\partial \mathbf{u}} = \frac{1}{h_i} \frac{\partial}{\partial \mathbf{u}} \mathbf{n}_i^T \mathbf{B}_i \mathbf{u} = h_i^{-1} \mathbf{n}_i^T \mathbf{B}_i. \tag{24}$$

Substituting from Eqs. (22) and (24) in Eq. (23) it is possible to obtain a nonlinear system of discrete equations with respect to displacements $\mathbf{u}$. The Newton-Raphson method can be used to solve this system. In order to do that we need to compute the tangent stiffness matrix

$$\mathbf{K}(\mathbf{u}) = \frac{\partial \mathbf{g}(\mathbf{u})}{\partial \mathbf{u}} = \frac{\partial}{\partial \mathbf{u}} \left(\frac{\partial V(\mathbf{u})}{\partial \mathbf{u}} \right)^T. \tag{25}$$

It is possible to get the closed form expression for the tangent stiffness matrix. Indeed, considering Eq. (12) we have

$$\begin{aligned} \mathbf{K}(\mathbf{u}) &= \frac{\partial \mathbf{g}(\mathbf{u})}{\partial \mathbf{u}} = \frac{\partial}{\partial \mathbf{u}} \left(\frac{\partial V(\mathbf{u})}{\partial \mathbf{u}} \right)^T \\ &= \sum_{i=1}^{N} \frac{\Delta S_i}{h_i^2} (\alpha_1 + 2\alpha_2 \varepsilon_i + 3\alpha_3 \varepsilon_i^2) (\mathbf{n}_i^T \mathbf{B}_i)^T (\mathbf{n}_i^T \mathbf{B}_i). \end{aligned} \tag{26}$$

It is useful to rewrite this matrix in a more compact form

$$\mathbf{K}(\mathbf{u}) = \sum_{i=1}^{N} c_i(\mathbf{u}) \mathbf{D}_i, \tag{27}$$

where

$$c_i(\mathbf{u}) = \frac{\Delta S_i}{h_i^2} (\alpha_1 + 2\alpha_2 \varepsilon_i + 3\alpha_3 \varepsilon_i^2). \tag{28}$$

$$\mathbf{D} = (\mathbf{n}_i^T \mathbf{B}_i)^T (\mathbf{n}_i^T \mathbf{B}_i). \tag{29}$$

The Newton-Raphson method for solution of Eq. (23) takes the following form

$$\begin{cases} \mathbf{K}(\mathbf{u}^{(n)}) \boldsymbol{\Delta}^{(n)} = -\mathbf{g}(\mathbf{u}^{(n)}) \\ \mathbf{u}^{(n+1)} = \mathbf{u}^{(n)} + \boldsymbol{\Delta}^{(n)} \\ n = 0, 1, \ldots, \quad \mathbf{u}^{(0)} = \mathbf{0} \end{cases} \tag{30}$$

The process can be terminated, for example, when

$$\frac{\left\| \mathbf{u}^{(n+1)} - \mathbf{u}^{(n)} \right\|}{\left\| \mathbf{u}^{(n+1)} \right\|} < \text{TOLERANCE} = 10^{-6}, \tag{31}$$

where the norm is defined for any vector $\mathbf{a}$ as $\|\mathbf{a}\| = \sqrt{\mathbf{a}^T \mathbf{a}}$.

Since the contact area under the reactive load is unknown, a much larger area available for the contact between the two adjacent bodies is assumed to initiate the calculation. If any of the springs are carrying tensile force compared to the unloaded state, these springs are eliminated from the contact area and the same calculation will be repeated again using the convergence criterion stated above. Even with the required iterative process, large number of springs to be considered and the non-linear simultaneous algebra equations to be solved, the entire computation and results display can be handled by a PC computer with only small amount of CPU time.

4 Applications discrete element analysis (DEA) model

In the equivalent joint contact stress DEA model, there were three types of interface springs: 1) compression resistance and tension break spring, 2) tension resistance compression break spring, and 3) shear spring, with types 1 and 2 being normal springs. Normal springs were placed at the centroid of each area grid and normal to the contact surface usually on the concave side of the joint or along the ligament or tendon tension fiber direction. Although joint frictions are usually ignored, shear springs could be inserted in two orthogonal directions parallel to joint contact surface to simulate degenerated or prosthetic replaced joints. In the joint model, muscles are not included in the unknowns since their contractile forces would have been determined together with the joint constrain force (including the contact forces) which are considered as the nodal reactions to be used to calculate the joint contact pressure and ligament tension. Relative displacements of the rigid bodies are defined as the translational and rotational deviations compared to its unloaded state in reference to Cartesian coordinate system about the body centroid. In certain conditions, bone-implant component interface stresses and micro-motion can also be approximated (Ide et al., 1989). Many applications both in 2D and 3D models have produced useful biomechanical information for basic science and clinical applications (Horii, et al., 1990; Hsu, et al., 1990; Ide, et al., 1989; Shiba N., 1991; Schuind, et al., 1995; Genda, et al., 2001; Iwasaki, et al., 1998a, 1998b). To illustrate the utility and versatility of the DEA technique in musculoskeletal biomechanics, two application examples of different context are given here.

4.1 Simplified 2D Hip Stem-Bone Interface Stress and Micro-motion Analysis

The metal stem and femur bone in a non-cemented hip replacement procedure were treated as two-dimensional, 10-mm thick rigid elements in contact through the interfaces. If the thickness of the stem varies, the stiffness value of the interface spring elements in each region could be adjusted proportionally using the contact area projection method (Fig. 4) (Schuind et al., 1995). A side re-enforcing plate was assumed so that the cortical walls could move as a single rigid body. For comparison purpose, an equivalent FEM model was created using gap elements at the interface (Fig. 5). In the DEA model (Fig. 6), compression resistance tension break normal springs and shear springs were placed at 1 mm interval along the contact line to simulate the interface condition in a non-cemented stem during the post operative period before tissue bonding or bone in-growth occurs. The deformation of the elastic springs due to the rigid body displacement of the stem in reference to the bone was used to calculate the compressive and shear interface stresses based on the assumed or reported interface material properties (Ide, et al., 1991).

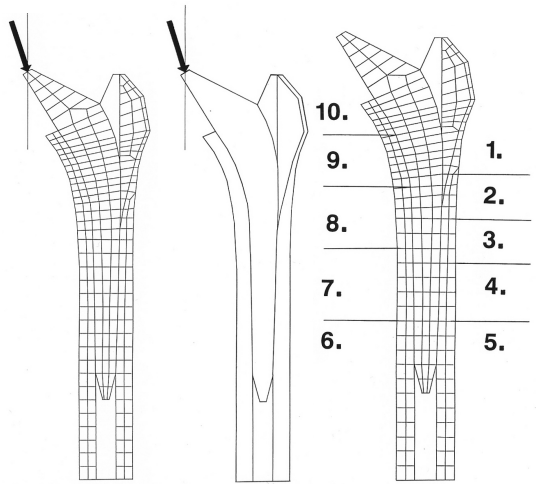

Figure 5: The identical two-dimensional hip replacement model used to compare bone-stem interface normal stress. (a) The FEM with re-enforcing side plate. (b) The DEA while the cortical bone will be moved as a single rigid body. (c) The ten zones of interest used to compare the bone-stem interface stresses predicted by both methods.

A load of 3000N (about four times body weight) was applied at an angle of 15 degrees inclined laterally to the center of the pelvis to simulate the single stance loading during gait (Crowninshield, et al., 1978; Huiskes, et al., 1990) with the dis-

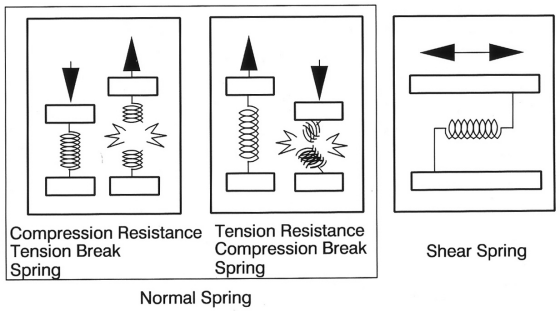

Figure 6a: The interface spring types used in the DEA technique. Definitions of the "compression resistance" and the "tension resistance" normal springs and the shear spring elements.

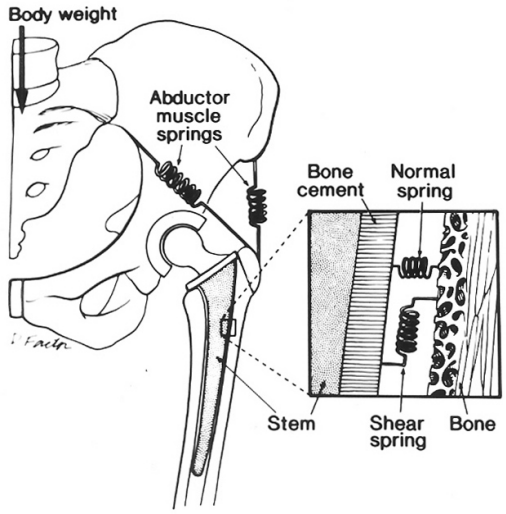

Figure 6b: The interface spring types used in the DEA technique. Schematic diagram of the hip model in which DEA is used to determine bone-stem interface stresses. The tendon/muscle surrounding the joint are modeled as tensile springs.

tal end of femur rigidly fixed. The stiffness property of the gap elements for the FEM and stiffness property for the spring unit of the DEA were made similar (FEM: K_n=200,000 Mpa, K_s=0 Mpa, μ=0, DEA: k_d=200,000 N/mm/unit, k_s=0 N/mm/unit). Since the density of the gap elements in the FEM model did not match that of the spring elements in DEA model (1 spring/mm), interface stresses were summed according to ten zones of interest through out the interface to facilitate direct comparison between the results from the two methods. In order to provide an overall comparison of the methods and to assess the effect of modeling parameter, the root-mean-square values (RMS) of the differences for each of the ten interface zones were used.

The corresponding normal compressive stress summation for each of the ten interface zones for the two methods were presented under different shear resistance (Table 1). The results were similar at zones "1", "2", "4", "6", "9" and "10", and the differences between the corresponding values were less than 20%. The DEA method tended to over-estimate compressive stresses in zone "3" and under-estimate the interface stresses in zones "5", "7" and "8". In general, the two methods compared favorably and these results were not affected by the interface shear resistance conditions. In the zones "5", "7" and "8", DEA method predicted interface separation condition (normal stress summation less than 0.5 MPa) while using FEM method, only zone "8" had a tendency to become separated especially under high interface shear resistance.

In frictionless case (k_s, K_s=0, μ=0), the root-mean-squares value of the differences between the FEM and DEA results for each of the corresponding ten zones was 8.144. The largest compressive stresses were observed in the same zones (zones "10" and "1") and their numerical values were similar. Large differences (>20%) in absolute values between the two methods occurred only in zones "3", "5" and "7". At the middle-medial region (zones "7" and "8") and the disto-lateral region (zone "5") of the interface, relatively high stresses were found in FEM results, but not in RBSM results. The reverse was true only in the mid-lateral region (zone "3") (Fig. 7). The differences between the two methods in predicting stem/bone interface normal stresses were independent to the assumed shear resistance in each model (Table 1).

In addition to the change of interface conditions related to shear resistance, changing the normal stiffness property for the FEM gap element was also investigated. Estimated values based on the averaged stiffness properties of the adjacent elements across the gap were tried (Rizzo, A. R.,

Table 1: Comparison of bone-stem interface normal stresses determined by DEA (Discrete Element Analysis) and FEM methods under different gap stiffness properties (k_d=200,000 N/mm/unit; K_n=200,000 MPa)

Compressive Stress, $\boldsymbol{\sigma}_n$ (MPa)

	DEA	FEM	DEA	FEM	DEA	FEM
* Zone of Interest	k_s=0	K_s=0 $\mu = 0$	k_s=1000	K_s=1000 $\mu = 0.05$	k_s=2000	K_s=2000 $\mu = 0.11$
1	10.55	9.91	8.18	8.12	6.60	6.87
2	9.84	9.32	7.79	7.51	6.43	6.24
3	7.90	2.71	6.44	2.15	5.45	1.76
4	3.94	3.46	3.46	2.72	3.13	2.21
5	0.21	4.25	0.33	3.43	0.46	2.84
6	4.77	3.91	3.24	2.99	2.24	2.35
7	0.51	4.64	0.18	3.59	0.07	2.86
8	0	1.50	0	1.12	0	0.85
9	7.72	8.74	6.49	6.53	5.67	5.02
10	17.32	16.36	14.39	13.86	12.42	12.13
** RMS Value	8.14		6.47		5.41	

** $\sqrt{\sum_{i=1}^{10}[(\sigma DEA)\,i-(\sigma FEM)\,i]^2}$, where i=zone number

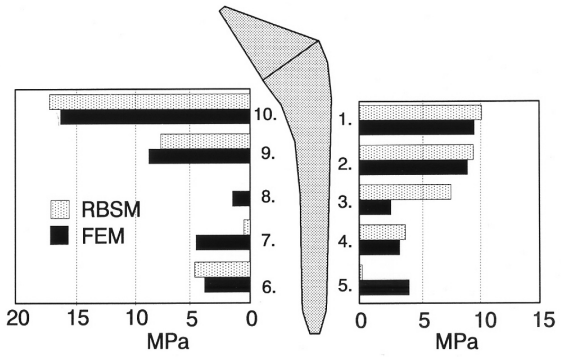

Figure 7: Comparison of the interface normal stresses between the bone and the stem determined from the FEM and DEA (Rigid Body Spring Model) technique in the ten zones of interest under the interface stiffness conditions: K_n,k_d, =200,000 Mpa, N/mm/unit respectively; K_s, k_s=0; μ=0.

1991), decreasing the normal stiffness property of the gap elements caused reduction of the normal stresses in all zones was found. On the other hand, increasing normal stiffness for the gap elements for the FEM method increased the magnitudes of the normal interface stresses but at a reduced rate and finally stabilized at approximately 100-fold of K_n value increase. However, the relative changes in compressive stresses in the DEA model maintained their general trend regardless of the change of k_d values. The relative differences in interface stresses between the two methods under different loading condition remained small.

4.2 3D Hip Joint Contact Pressure in Activities of Daily Living

Intrinsic pathomechanical changes in articular cartilage and subchondral bone depend upon local stress levels rather than global joint loading. To estimate joint contact area and peak value distribution in the hip joint under daily activities may not be significant in determine femoral prosthesis stem and bone stresses, it will be essential to predict joint disease progress for patient management, preoperative planning and postoperative rehabilitation. This loading data when inverted onto the femoral head can also provide the biomechanical rationale for subchondral bone collapse and method of reconstruction under osteonecrosis conditions. Unfortunately, such data is not available in the current literature. In vitro studies to quantify contact pressure of the hip joint have been performed but the methods used were inappropriate for in vivo studies. Numerical sim-

ulation technique and a radiograph-based joint model combined with measured joint loading data in living subjects with instrumented prosthesis are ideal for population based studies as well as for analyzing individual patient. This application used the Discrete Element Analysis (DEA) technique on a realistic joint model to predict hip contact area and pressure distribution based on the in vivo joint motion and force data during activities of daily living (ADL).

By assuming a spherical shape of the femoral head, a geometrical model was created from an anteroposterior (AP) radiograph of a subject's hip joint (Genda et al., 2003). In the radiograph, contour line of the femoral head was digitized and the radius and center of the best-fit circle were calculated using the acetabular sourcil line and a least square fit method. Anterior and posterior edges of the acetabulum were then digitized on the radiograph. This approximated joint surface of contact on the acetabulum was divided into approximately 4000 rectangular mesh elements. The joint surface was assumed to be congruent. The trend in pressure distribution in the hip joint during ADL was captured (Yoshida et al., 2005).

At the center of each mesh element, one compressive spring was placed normal to the opposing mesh of the femoral head surface. The stiffness property of the linear springs was determined from the cartilage Young's Modules of 11.85 MPa (Kempson, 1980), Poisson ratio of 0.45 (Blankevoort et al, 1991) and thickness of 2.66 mm (Athanasiou et al., 1994). The joint shear resistance was ignored due to the extremely low friction of the cartilage. Since the majority of the joint deformation under load occurs in the acetabulum and femoral head cartilage, the underlying subchondral bone structures were assumed rigid. The rigid body displacement field provided the deformation of the springs which approximated the joint contact area and pressure. Hip joint motion and joint contact forces during ADL were taken from Bergmann et al (2001), which was based on the in vivo measurements in patients with instrumented hip replacement prosthesis. The graphic animation feature of the simulation software, VIMS (Virtual Interactive Musculoskeletal System) (Chao, 2003) was used to display the analysis results for visualization purpose.

The acetabulum available contact area was divided into four regions to ease the description of the location of the peak pressure (Fig. 8a). In normal walking, the maximum contact pressure was relatively low due to the large area of joint contact throughout the gait cycle (Fig. 8b). The magnitude and occurrence of the peak contact pressure coincided with that of the ground reaction force during gait cycle for different walking speed. In stair walking, the peak pressure going upstairs (5.71 MPa), was higher than that in going downstairs (3.77 MPa) although the measured joint contact force magnitudes were in opposite order. During the closed kinetic chain activity, the hip peak contact pressure was moderate (3.65 MPa). The highest joint contact pressure occurred during sitting down on a chair (9.36 MPa) or standing up from it (8.97 MPa) mainly due to the small contact area at the edge of the posterior horn of the acetabulum. The peak pressure, the contact area, the activity cycle percentage and the joint contact force data of all ADL are tabulated in Table 2.

The maximum hip contact force and the maximum pressures generally occurred at the same time during the gait activity. The magnitude of the contact pressure, however, depends on the direction of the contact force acting on the acetabulum, which determines the size of the contact area (Fig. 9). During "sitting down on chair", the highest pressure among all activities, was observed at the edge of the posterior horn with a small area of contact. In addition, the "descending stairs" was thought to be more pressure-bearing than the "ascending stairs" due to higher contact force. However, the maximum contact pressure was actually higher in "ascending stairs" because of the smaller joint contact area involved. These explain why patients with hip joint problems cannot manage stair walking, sitting down and getting up from low chairs easily.

5 Discussion

In musculoskeletal biomechanics, determination of the load born by the system components un-

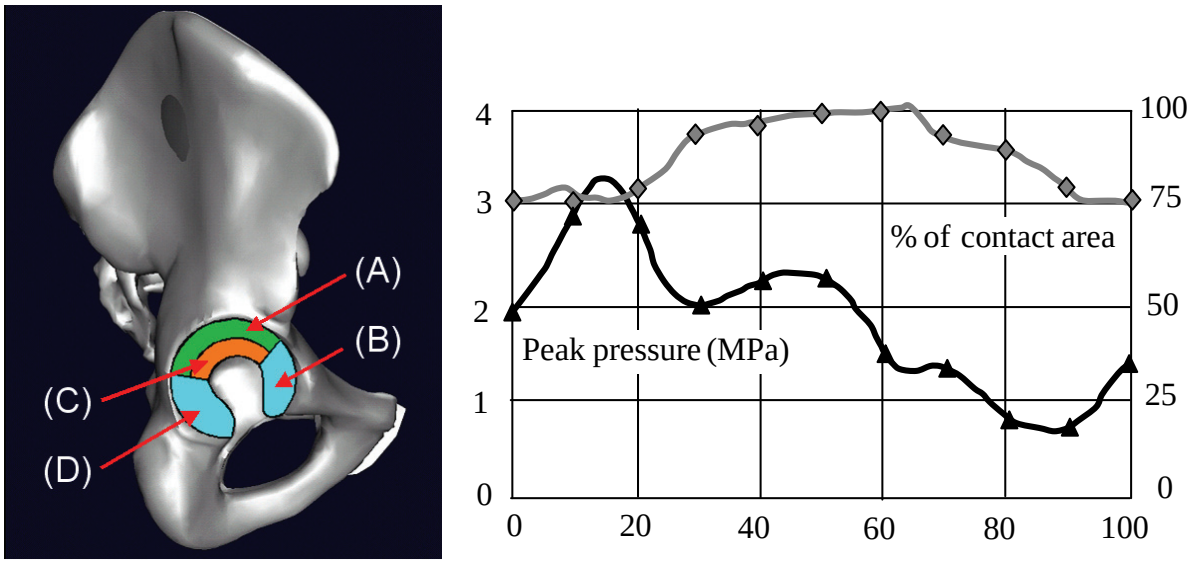

Figure 8: a. Definition of hip joint acetabulum contact regions: (A) Lateral roof; (B) Anterior horn; (C) Medial roof; (D) Posterior horn. b. Peak contact pressure and area during normal gait cycle.

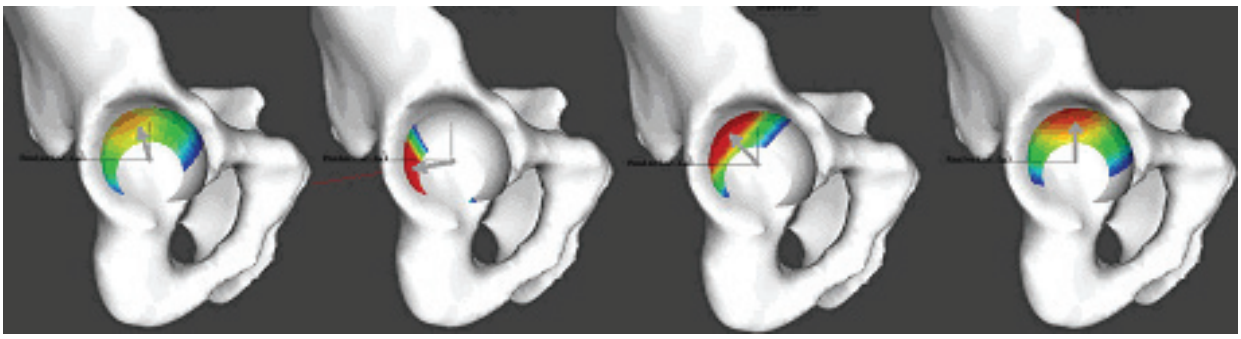

Figure 9: The maximum hip joint pressure distribution during activities of daily living. The white arrow indicate the joint resultant contact force vector. A. Normal walking; B. Sitting down to a chair; C. Ascending stairs; D. Descending stairs.

Table 2: The hip joint peak pressure and location, contact area, incidence of occurrence during the cycle of activity, and the contact force magnitude in various activities of daily living.

Activities of Daily Living	Peak Pressure (MPa)	Contact Area (% total area)	Activity Cycle (%)	Contact Force (%BW) (5)
Fast Walking	3.28 (Lateral Roof)	78.7	12.5	274
Normal Walking	3.24 (Lateral Roof)	76.3	16.5	234
Slow Walking	2.87 (Lateral Roof)	81.2	16.0	243
Standing up	8.97 (Posterior Horn)	19.7	35.0	179
Sitting down	9.34 (Posterior Horn)	17.6	50.5	148
Knee Bending	3.65 (Posterior Horn)	51.6	53.0	140
Up stairs	5.71 (Lateral Roof)	52.1	11.0	260
Down stairs	3.77 (Lateral Roof)	80.6	55.0	314

der the static and dynamic conditions is the origin and foundation of the rest of the scientific endeavors in this field. There is an analogy in the history of mechanics where the classical mechanics was the first to be developed as it could be traced back to the era of Galileo and Newton in the 17^{th} century. Although Robert Hooke was recognized to be the first with the notion of elasticity, this branch of mechanics blossomed much later in time. With the introduction of the electromagnetic field theory and radiation energy, particle and quantum mechanics begun to excel from the late 19^{th} century to the early 20^{th} century. With the periodic improvements of the experimental and theoretical (or numerical) methods while taking the advantage and stimulation from other related fields, each branch of mechanics seeks its own advances and applications making what our current technology is today. Whether the field of musculoskeletal biomechanics will follow the same cyclic course of development will remain to be seen. However, each branch of this field must be advanced in a compatible and coordinated manner to maintain their validity within the framework of biological system's structure and function. This requires balanced resources both in manpower and research funding.

It is true that the establishment of the discipline of bioengineering in general and biomechanics in specific, has brought us enormous excitement and inspiration not mentioning many landmark applications. Those who worked in the field of musculoskeletal biomechanics full-time have also experienced countless frustrations and disappointments. Relatively speaking, neither engineering nor mechanics shall lead the fields of medicine, surgery, and biology just as engineering and applied mechanics have not dictated the fields of physics, mathematics, and chemistry. However, engineering has and will facilitate the crucial advancements in these biomedical fields and transform scientific breakthroughs into practical bedside applications with the required effectiveness, reliability and affordability. It is with this spirit this paper was written.

In predicting the loading and deformation of biological tissue, organ and system, it is rarely if not impossible to discuss the exact solution as practiced in various engineering technologies. Even in biological fields, nothing can be truly regarded as absolute since each patient and his/her disease or tissue degeneration involvement are different although all could be classified in the same diagnosis criterion. In the common engineering grading of safety and reliability described in the famous Sigma-6 scale, all medical related treatments are in the lower ranks due to many uncontrollable factors where natural variability and unpredictable mutations at the sub-molecule level are something beyond the control of physical laws. In addition, countless assumptions and simplifications have been adapted in the model and analysis process. Hence, the effort of biomechanics must be judiciously balanced with reality, practicality, the time and economic constraints. Although the DEA technique has several limitations and drawbacks, it does provide the needed information efficiently and reliably for individual patient and situation to offer relevant clinical application to satisfy the medical counterpart.

Validation of the DEA technique was performed in several occasions using FEM models as demon-

strated in the first example in determining the stem-bone interface stress. Additional validation on the contact stress was conducted using the classic Hertzian problem solution using the analytical method, FEM and the combination of FEM and DEA technique (Shih et al, 1993, Stone et al, 1996a, 1996b; Li et al., 1997).

To analyze THR, various gap elements were used to simulate different interface conditions between prosthesis and bone, prosthesis and cement, and cement and bone (Harrigan, et al., 1991; Keaveny, T. M., 1992; Ebramzadeh, et al., 1992). However, to exactly define the interface behavior using proper gap elements in FEM is a rather complex problem. Rizzo (1991) attempted to illustrate these problems using simple four nodes FEM model. Usually the stiffness of the gap elements was recommended to have a magnitude one to two order greater than the adjacent element at the gap. If the stiffness of the gap element was too small, the error became bigger since the displacements of the contacting surface would become large and deformed. If the gap element became stiffer, then the results would be more accurate, but longer computational time will be required due to the iterative processes in order to satisfy the equilibrium condition. Too large a stiffness value for the gap element could cause a "bouncing phenomenon" and stable results would be difficult to obtain. For these reasons, the number of computational iterations was set at ten.

When the gap element stiffness value increases for the FEM technique, the root-mean-squares values between the two methods decreased which indicates that stiffer gap element made FEM interface stress results behaved more like that in the DEA. However, the number of computational iterations for FEM was also significantly increased in order to allow the results to converge. Although such manipulation appeared to only adjust the behavior of the FEM results, this might provide a proper guide for the selection of interface spring stiffness for the DEA. These data support the rationale in using the DEA technique for interface stress assessment in non-cemented stem fixation condition. Previously published data on non-cemented fixation models (Barich, et al., 1995; Thanner, et al., 1995) provided convincing evidence on the magnitude of the micro-motion at the implant/bone interface to justify the DEA technique.

Although DEA could only provide implant-bone interface stresses and micro-movement, the ease of providing the model and conducting the analysis makes it more suitable for clinical application as a preoperative planning tool to optimize implant selection and placement. It is also an ideal tool for parametric analysis to consider geometry, interface condition and material changes in implant design. DEA technique can easily be extended for full three-dimensional implant-bone interface stress analysis similar to that used at the knee joint for contact stress analysis (Blankevoort, et al., 1991). With the aid of computer graphic presentation and visualization of the model and results in a simulation environment (Chao, 2003), wide and robust application of DEA technique in joint replacement surgery is highly anticipated.

Intrinsic loading to the joint surface is more problematic to the cartilage and subchondral bone degeneration. In prescribing daily activity limitation and rehabilitative exercises in patients with hip diseases or after reconstructive procedures, the present information will provide the biomechanical rationale to prolong treatment effects and minimize complications. As discussed before, there is really no way to determine how accurate the data generated are in an *in vivo* situation. Validation of the DEA technique was performed in several occasions using FEM models as demonstrated in the first example in determining stem-bone interface stress. Additional validation on contact stress determination was conducted using the classic Hertzian problem solution using the analytical method, FEM and the combination of FEM and DEA technique which produced very similar solutions (Shih et al, 1993, Stone et al, 1996a, 1996b; Li et al., 1997). The hip joint contact application as presented above, the input loading and motion data were obtained from patients wearing instrumented prosthesis which would be considered as highly acceptable. However, in normal person engaged in daily activities,

the present data would be somewhat in the lower bond of the solutions obtained. More effort needs to be devoted to predict muscle and joint loading based on improved model, kinamatic and external loading measurements, and the computational algorithm to deal with the redundant problem on hand. How important is it to consider the non-linear DEA models in analyzing joint dynamic loading especially for the transient stage requires further investigation. Should such consideration be proven essential, the general framework of the discrete element concept could be expanded to include fluid transport effect in the joint cartilage under loading.

The DEA technique can add the robustness of the biomechanical analysis software to determine joint contact and interface stress between bone and artificial implants. With combination of the VIMS software platform (incorporated in the computational toolbox), the power of biomechanical analysis at the tissue and structural level can become more attractive and thus draw increased competitiveness in getting research funding and the attention from our clinical counterpart. Certain validation experiments will be important to further establish the strength and limitations of this method. Very like what Professor Kawai had attempted in conducting non-linear analysis of solid and fluid systems without the use of finite element analysis. However, these two methods can be combined to offer the best tool to provide useful and improved data without suffering the drawbacks in either one. Finally, absolute solution in biological system is a wishful thinking but performing parametric analysis to generate comparative data which will be very useful both in basic science and clinical applications. It is worthwhile to remind the bioengineers again that engineering and mechanics, though serving as very powerful catalyst and enhancer, will not be the driving force either in medicine or biology.

Acknowledgement: The authors would like to express their profound respect and best wishes to Professor YC Fung, who, among only a handful of others, has made the discipline of biomechanics what it is today. There are several significant contributors to promote the EDA technique we would like to acknowledge including Professor Kawai, Professor KN An, Dr. Himeno, Dr. Tsumura, Dr. Genda, Professor GA Li, Professor Sakamoto, Dr. Horii, Professor F Schuind and others. Among them, we would like to especially pay tribute to Professor James Stone who passed away in October of 2007. He provided the definitive validation of the DEA and the DEA-FEM combination techniques to solve various contact problems in the light of the classic Hertz solution. The non-technical statements expressed in this paper concerning biomechanics and bioengineering are entirely the authors' provocative opinions which do not represent that of other DEA users or any of our close collaborators.

References

1. An, K.N., Himeno, S., Tsumura, H., Kawai, T., Chao, E.Y.S.: Pressure Distribution on Articular Surfaces: Application to Joint Stability Evaluation. J. Biomechanics, Vol. 23, pp. 1013-20, 1990.

2. Ateshian, G.A., Lai, W.M., Zhu, W.B., and Mow, W.C., 1994. An asymptotic solution for the contact of two biphasic cartilage layers. Journal of Biomechanics 27, 1347-1360.

3. Ateshian, G.A., Wang, H., 1995. A theoretical solution for the frictionless rolling contact of cylindrical biphasic articular cartilage layers. Journal of Biomechanics 28, 1341-1355.

4. Ateshian, G.A., Warden, W.H., Kim, J.J., Grelsamer, R.P., and Mow, W.C., 1997. Finite deformation biphasic material properties of bovine articular cartilage from confined compression experiments. Journal of Biomechanics 30, 1157-1164.

5. Athanasiou, K.A. Agarwal, A. Dzida, F.J., 1994. Comparative study of the intrinsic mechanical properties of the human acetabular and femoral head cartilage. Journal of Orthopaedic Research 12, 340-349.

6. Barich, F. C., Brown, T. D., Callaghan, J. J.: Effect of Proximal and Distal Fit on Micromotion of An Uncemented Femoral Component under Realistic In Vivo Gait Loads. ORS Proceedings, p. 268, Feb., 1995.

7. Bergmann, G. Deuretzbacher, G. Heller, M. Graichen, F. Rohlmann, A. Strauss, J. Duda, G.N., 2001. Hip contact forces and gait patterns from routine activities. Journal of Biomechanics 34, 859-871.

8. Blankevoort, J.H., Kuiper, R., Huiskes, R., Grootenboer, H.J.: Articular Contact in a Three-Dimensional Model of the Knee. J. Biomechanics Vol. 24, pp. 1019-31, 1991.

9. Brown, T.D., DiGioia, A.M.: A Contact-Coupled Finite Element Analysis of the Natural Adult Hip. J. Biomechanics, Vol. 17, pp. 437-448, 1984.

10. Chao, E.Y.: Graphic-based musculoskeletal model for biomechanical analysis and animation. Journal of Med Eng Physics, 4:3:1, 687-699, 2003.

11. Crowninshield, R.D., Johnston, R.C., Andrews, J.G.: A Biomechanical Investigation of the Human Hip. J. Biomechanics, Vol. 11, pp. 75-85, 1978.

12. Ebramzadeh, Z.L.E., Mckellop, H., Zahili, C., Sarmiento, A.: The Influence of the Stem-cement Bonding Strength of the Cement Stresses in Total Hip Arthroplasty. ORS Proceedings, p. 377, March, 1992.

13. Harrigan, T.P., Harris, W.H: A Three-dimensional Non-linear Finite Element Study of the Effect of Cement-prosthesis Debonding in Cemented Femoral Total Hip Components. J. Biomechanics, Vol. 24, pp. 1047-1058, 1991.

14. Genda E, Iwasaki N, Li GA, MacWilliams BA, Barrance PJ, Chao EYS: Normal Hip Joint Contact Pressure Distribution in Single-leg Standing – Effect of Gender and Anatomic parameters. J of Biomechanics, Vol. 34, pp 895-905, 2001.

15. Horii, E., Garcia-Elias, M., An, K.N., Bishop, A.T., Cooney, W.P., Linscheid, R.L., Chao, E.Y.S.: Effect on Force Transmission Across the Carpus of Procedures Designed to Treat Kienbock's Disease. An analytic study. J. Hand Surg., Vol. 15-A, pp. 393-400, 1990.

16. Hsu, R.W.W., Himeno, S., Coventry, M.B., Chao, E.Y.S.: Normal Axial Alignment of the Lower Extremity and Load-Bearing Distribution at the Knee. Clin. Orthop., Vol. 255, pp. 215-27, 1990.

17. Huang, C.-Y., Stankiewicz, A., Ateshian, G.A., Mow, V.C., 2005. Anisotropy, inhomogeneity, and tension-compression nonlinearity of human glenohumeral cartilage in finite deformation. Journal of Biomechanics 38, 799-809.

18. Huiskes, R.: The Various Stress Patterns of Press-Fit, Ingrown, and Cemented Femoral Stems. Clin. Orthop. Vol. 261, pp. 27-38, 1990.

19. Ide, T., Akamatsu, N., Hamada, Y., Nakajima, I., Yamamoto, Y., Tatsuki, S., Amano, T.: Non-linear Stress Analysis of Various Kinds of Cementless Total Hip Systems. Jpn J Artif Organs, Vol. 18, pp. 356-359, 1989.

20. Ide, T., Yamamoto, Y., Tachiki, S., Akamaysu, N., Chao, E.Y.S.: Determination of Spring Constants for the Rigid Body Spring Model. J Jpn Orthop Biomech, Vol. 12, pp. 125-131, 1991.

21. Iwasaki, N., Genda, E., Minami, A., Kaneda, K., Chao, E.Y.S.: Force Transmission Through the Wrist Joint in Kienbock's Disease. J. of Hand Surgery, Vol. 23A, No. 3, May, 1998.

22. Iwasaki, N., Genda, E., Barrance, P.J., Minami, A., Kaneda, K., Chao, E.Y.: Biomechanical analysis of limited intercarpal fusion for the treatment of Kienbock's disease: a three-dimensional theoretical study. J. Orthop. Res. 16: 256-263, 1998.

23. Kawai, T.: A New Element in Discrete Analysis of Plane Strain Problems. Seisan Kenkyu, Vol. 29, pp. 204-207, 1977.

24. Kawai, T., Toi, Y.: A New Discrete Analysis on Dynamic Collapse of Structures. J. Society of Naval Architects of Japan, Vol. 143, pp. 275-281, May, 1978.

25. Kawai, T., Takeuchi, N.: A Discrete Method of Limit Analysis with Simplified Elements. ASCE Int. Conf. Comp. Civil Engng., New York 1981.

26. Kawai, T., Watanabe, M.: Discrete Analysis of Incompressible Viscous Flow Problem by Means of New Lower Order Triangular Element. Chap. 5, Finite Element in Fluids, Vol. 5 (Ed.: Gallagher, Oden, Zienkiewicz, Kawai, Kawahara), John Wiley & Sons, New York, 1984.

27. Keaveny, T.M.: Relative Motion for a Moor-Type Cementless Hip Prosthesis in the Early Post-Operative Situation. ORS Proceedings, p. 379, March, 1992.

28. Kempson, G., 1980. The Mechanical Properties of Articular Cartilage. In: The Joints and Synovial Fluid 2. New York Academic Press, 177-238.

29. Lewis, J.L., Askew, M.J., Wixson, R.L., Kramer, J.M., Tarr, R.R.: The Influence of Prosthetic Stem Stiffness and of a Calcar Collar on Stresses in the Proximal End of the Femur with a Cemented Femoral Component. J Bone Joint Surg, Vol. 66-A, pp. 280-286, 1984.

30. Li, G. Sakamoto, M. Chao, E.Y., 1997. A comparison of different methods in predicting static pressure distribution in articulating joints. Journal of Biomechanics 30, 635-638.

31. Mow, V.C., Kuei, S.C., Lai, W.M., Armstrong, C.G., 1980. Biphasic creep and stress relaxation of articular cartilage in compression: theory and experiment. Journal of Biomechanical Engineering 102, 73-84.

32. Mow, V.C. and Ratcliffe, A.: Structure and Function of Cartilage and Meniscus. Chap. 4, pp. 113-177, Basic Orthopaedic Biomechanics, 2^{nd} Ed. (Ed.: Mow and Hayes), Lippincott-Raven, 1997.

33. Rizzo, A.R.: FEA Gap Element; Choosing the Right Stiffness. Mech. Engng., Vol. 113: 57-59, 1991.

34. Schuind, F., Cooney, W.P., Linscheid, R.L., An, Kn., Chao, E.Y.S.: Force and Pressure Transmission through the Normal Wrist. A Theoretical Two-dimensional Study in the Posteroanterior Plane. J. Biomechanics, Vol. 28, pp. 21-36, March, 1995.

35. Shih, J.S., Ju, S.H., Rowlands, R.E., An, K.N., Chao, E.Y.S.: Analysis of frictional joint contact. BED-Vol. 26, Advances in Bioengineering, ASME, pp. 51-54, 1993.

36. Shiba, N.: Biomechanics of Chiari Pelvic Osteotomy. J Jpn Orthop Asso., Vol. 65, pp. 337-348, 1991.

37. Stone, J.J.S., Ju, S.H., Chao, E.Y.S., Morrey, B.F., An, K.N.: Analysis of Articular joint contact by an efficient finite element method. Developments in Theoretical and Applied Mechanics, vol. 18, pp. 476-482, 1996.

38. Stone, J.J.S., Ju, S.H., Chao, E.Y.S., Morrey, B.F., An, K.N.: Efficient finite element method for contact analysis of articular joints. BED-Vol. 33, Advances in Bioengineering, ASME, 427-429, 1996.

39. Thanner, J., Malchau, H., Karrholm, J., Herberts, P., Wesslen, B.: Increased Micromotions of Hip Prostheses Inserted with Cold-curing Bone Cement. A Roentgen-stereophotogrammetric Study. ORS Proceedings, p. 714, Feb., 1995.

40. Volokh, K.Y., Chao, E.Y.S., Armand, M.: On foundations of discrete element analysis of contact in diarthrodial joints. Molecular and Cellular Biomech. Vol.4, pp. 67-74, 2007.

41. Yoshida H, Faust A, Wilckens J, Kitagawa M, Fetto J, Chao EYS: Three-dimensional dynamic hip contact area & pressure distribution during activities of daily living. J. Biomech., Vol. 38, pp. 1-9, 2005.